



Interannual Variability and Multiyear Trends of Sea Surface Salinity in the Amazon-Orinoco Plume Region From Satellite Observations and an Ocean Reanalysis

Nguyen Dac Da¹  and Gregory R. Foltz² ¹VNU University of Science, Vietnam National University, Hanoi, Vietnam, ²Atlantic Oceanographic and Meteorological Laboratory (AOML), National Oceanic and Atmospheric Administration, Miami, FL, USA**Key Points:**

- Horizontal advection influenced by the North Atlantic Oscillation (NAO) is the main driving force for plume interannual variability
- The NAO and El Niño Southern Oscillation (ENSO) are the ultimate drivers of plume salinity in the flood and dry season, respectively
- Plume salinity shows a significant positive trend during 2010–2016 when NAO and ENSO transitioned from a negative to a positive phase

Supporting Information:

Supporting Information may be found in the online version of this article.

Correspondence to:G. R. Foltz,
gregory.foltz@noaa.gov**Citation:**Da, N. D., & Foltz, G. R. (2022). Interannual variability and multiyear trends of sea surface salinity in the Amazon-Orinoco plume region from satellite observations and an ocean reanalysis. *Journal of Geophysical Research: Oceans*, 127, e2021JC018366. <https://doi.org/10.1029/2021JC018366>Received 20 DEC 2021
Accepted 13 APR 2022

Abstract The Amazon and Orinoco Rivers form the largest river system on Earth with wide-reaching impacts on the biophysical climate of the region. Based on 11 years of satellite observations, here we show strong interannual variability of sea surface salinity (SSS) in the plume region that is about three times larger than in the surrounding region. This variability has been driven mainly by changes in horizontal advection of the plume with smaller contributions from precipitation, river discharge, and vertical mixing. Interannual variability of horizontal advection occurs mainly near the eastern boundary of the plume region and especially in the latitude range of the North Equatorial Countercurrent (3°–10°N). The North Atlantic Oscillation (NAO) and El Niño Southern Oscillation (ENSO) strongly modulate SSS in the plume region during the boreal spring-summer (flood) and fall-winter (dry) seasons, respectively, through their impacts on the tropical North Atlantic Ocean circulation. Overall, the NAO exerts a stronger influence on plume SSS than ENSO. The plume SSS also shows a significant upward trend during 2010–2016, corresponding to transitions of the NAO and ENSO from negative to positive phases. This was followed by a downward trend during 2017–2020 when both the NAO and ENSO decreased from their 2015–2016 peaks. These results show that year-to-year changes in the spatial mean SSS of the Amazon-Orinoco plume are driven mainly by large-scale climate forcings and their associated imprints on tropical Atlantic Ocean circulation and very little by changes in river outflow and associated rainfall over land.

Plain Language Summary About 200,000 m³ of fresh water per second is discharged into the tropical North Atlantic by the Amazon and Orinoco Rivers, creating a large low-salinity plume that sometimes exceeds a million km². The plume is often more turbid and stable than surrounding waters and can trap more heat from solar radiation, triggering atmospheric convection that can increase rainfall over the Caribbean Sea and Central America and strengthen tropical cyclones. Here, we find strong interannual variability of surface salinity in the Amazon-Orinoco plume region over the 2010–2020 satellite period. Additional data from an ocean reanalysis reveal that interannual variability of the plume is mainly driven by large-scale ocean circulation, which in turn is driven by large-scale climate phenomena: El Niño Southern Oscillation (ENSO) in the dry season and the North Atlantic Oscillation (NAO) in the flood season. The plume surface salinity also shows a significant upward trend (i.e., weakening of the plume) during 2010–2016, corresponding to transitions of the NAO and ENSO from negative to positive phases.

1. Introduction

The Amazon and Orinoco Rivers combined account for about 20% of the global freshwater that is transported to the ocean via rivers (Hu et al., 2004). With a freshwater discharge peak of $\sim 3 \times 10^5$ m³/s, the Amazon-Orinoco river plume can reach more than 10⁶ km² in size (Grotsky et al., 2014) and significantly impact the dynamics and biogeochemical phenomena of the North Atlantic (Chérubin & Richardson, 2007; Hu et al., 2004; Varona et al., 2019; Vizy & Cook, 2010). The strong buoyancy of the surface freshwater in the river plume limits mixing, traps heat within the surface layer, and increases sea surface temperature (Varona et al., 2019; Vizy & Cook, 2010). With warmer sea surface temperature, the Amazon-Orinoco plume can affect Atlantic hurricane activity, the large-scale atmospheric circulation over the northwestern tropical Atlantic, and associated rainfall over the Caribbean Sea and Central America (Vizy & Cook, 2010). The freshwater input from the river plume also impacts the surface ocean circulation and eddies (Chérubin & Richardson, 2007; Varona et al., 2019), and

sea level in the tropical Atlantic (Giffard et al., 2019). The abundant nutrients associated with the freshwater flux can strongly impact ocean productivity in the plume and beyond (Gouveia et al., 2019; Subramaniam et al., 2008).

The Amazon-Orinoco river discharge has strong seasonality. Amazon outflow ranges from $10^5 \text{ m}^3 \text{ s}^{-1}$ in November to $2.4 \times 10^5 \text{ m}^3 \text{ s}^{-1}$ in June, whereas the Orinoco discharge ranges from $10^4 \text{ m}^3 \text{ s}^{-1}$ in March to $7 \times 10^4 \text{ m}^3 \text{ s}^{-1}$ in August (Figure S1 in Supporting Information S1). Combined, the two rivers discharge a minimum of $1.3 \times 10^5 \text{ m}^3 \text{ s}^{-1}$ in November and a maximum of $3 \times 10^5 \text{ m}^3 \text{ s}^{-1}$ in August. The mean Orinoco River discharge is about 15% of the Amazon's, but the Orinoco can contribute up to 25%–30% of the total Amazon-Orinoco discharge from August to October due to the seasonal phase shift between the two rivers.

In addition to the strong seasonality of river discharge, the strong western boundary currents in the northwestern Atlantic have strong impacts on the seasonal variability of the sea surface salinity in the plume region (Coles et al., 2013; Lentz, 1995) and more broadly in the northwestern basin (Foltz et al., 2004, 2015). The Amazon water is mainly transported northwestward to the Caribbean and North Atlantic in February–May by the North Brazil Current (NBC). From June to January, Amazon freshwater is carried by the NBC retroflection, which feeds the eastward North Equatorial Countercurrent (NECC) (Coles et al., 2013; Lentz, 1995; Muller-Karger et al., 1988). The Orinoco water mainly affects the eastern Caribbean (Lopez et al., 2013). The size of the Amazon-Orinoco river plume varies strongly throughout the year and is highly correlated with seasonal variations of river discharge (Zeng et al., 2008).

There have been studies reporting that North Atlantic climate variability is largely controlled by the North Atlantic Oscillation (NAO, George & Saunders, 2001; Hurrell & Deser, 2010) and El Niño Southern Oscillation (ENSO) (Ropelewski & Halpert, 1987; Tyaquicã et al., 2017; Zeng, 1999; Zeng et al., 2008). The NAO represents the variation of the meridional gradient of atmospheric pressure between the Azores high and the Icelandic low. The variation of atmospheric pressure in the Azores high also controls the variation of the meridional pressure gradient between the Azores high center and the tropical Atlantic (George & Saunders, 2001), which can affect the strength of trade winds in the tropical North Atlantic and associated mixing, evaporation, precipitation, and large-scale wind-driven ocean circulation. In addition, anomalous zonal atmospheric circulation associated with ENSO is known to strongly influence precipitation in the Amazon-Orinoco catchment and over the ocean where the rivers discharge (Enfield & Mayer, 1997; Ropelewski & Halpert, 1987; Zeng, 1999; Zeng et al., 2008).

Findings from previous studies also suggest strong interannual variability of the Amazon-Orinoco river plume and attribute it to multiple factors, such as river discharge (Molleri et al., 2010; Tyaquicã et al., 2017; Zeng et al., 2008), large-scale circulation (Coles et al., 2013; Foltz et al., 2015), eddies (Chérubin & Richardson, 2007; Fournier et al., 2017; Reverdin et al., 2021), wind, and ITCZ position (Fournier et al., 2017). Some of these studies use satellite ocean color to infer the variability of the Amazon plume (Hu et al., 2004). Besides the complication of separating colored dissolved organic matter (CDOM) and chlorophyll from surface reflectance, the variability of the plume water derived from ocean color is strongly affected by clouds and aliased by other phenomena, such as upwelling. Other studies use satellite SSS (Fournier et al., 2017; Grodsky et al., 2014) and ocean models (Coles et al., 2013) with limited time records of 2–4 years, which are too short to characterize interannual variability of the Amazon plume and its causes. In this study, we characterize the Amazon-Orinoco river plume interannual variability using an 11-year record of satellite observations. The causes of the variability of the plume are also determined using simple mixed layer salinity sensitivity analyses based on an ocean reanalysis, and connections to large-scale climate variability are investigated.

2. Methods

2.1. Data

We investigate variability of the Amazon-Orinoco plume using satellite observations of sea surface salinity and output from an ocean reanalysis. For satellite data, we use sea surface salinity data from the European Space Agency Sea Surface Salinity Climate Change Initiative Project (ESA CCI SSS, https://data.ceda.ac.uk/neodc/esacci/sea_surface_salinity/). In this product, level-2 and level-3 data from the SMOS, AQUARIUS, and SMAP missions are combined with corrections for land contamination, radio frequency interference, latitudinal dependence bias, and long-term bias. We use the monthly product version V03.21, which covers the period 2010–2020.

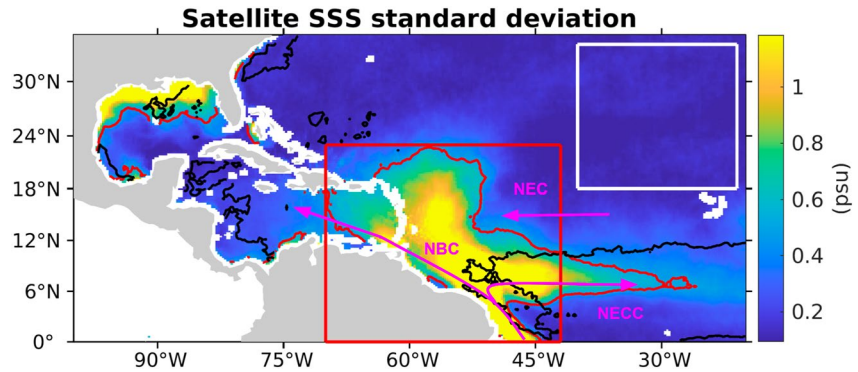


Figure 1. Tropical North Atlantic sea surface salinity variability over the 2010–2020 period obtained from satellite observations. The 0.5 psu standard deviation contour (in red) encloses the area in the upper 20% of sea surface salinity variability. The superimposed precipitation contour (in black, 5 mm/day) encloses the upper 20% of precipitation variability. The red rectangle defines the plume region for this study, and the white rectangle indicates a non-plume region used for comparison. The magenta arrows illustrate the North Brazilian Current, North Equatorial Current, and North Equatorial Counter Current.

To assess the role of different forcings in the variability of the plume, we use the Simple Ocean Data Assimilation (SODA) ocean reanalysis, version 3.4.2 (Carton et al., 2018). The forcings that can impact plume SSS include precipitation, evaporation, vertical mixing, and horizontal advection. Vertical mixing and horizontal advection can be inferred from SODA, but the SODA archive does not include precipitation and evaporation. We obtain these forcings directly from the ERA-Interim data set (Berrisford et al., 2011), which was used to force SODA (Carton et al., 2018). For river discharge, we obtained the Amazon River discharge data at Obidos station and Orinoco River discharge data at Ciudad Bolivar station from the HYBAM data set (available at <http://hybam.omp.obs-mip.fr/>).

To investigate the relationships between the plume's interannual variability and large-scale climate variability, we use the NAO index and Ocean Niño Index (ONI) produced by NOAA's Climate Prediction Center and distributed by NOAA's Physical Science Laboratory (<https://psl.noaa.gov/>). Both of these climate phenomena are known to strongly control the climate variability of the tropical Atlantic Ocean (Czaja et al., 2002; Enfield & Mayer, 1997).

2.2. Plume Index Computation

Previous studies have used different salinity thresholds to determine the plume extent, such as 34.7 psu (Zeng et al., 2008), 35 psu (Grotsky et al., 2014), or 35.5 psu (Fournier et al., 2017). In this study, we first define a region of high SSS variability that is bounded by the 0.5 psu SSS standard deviation contour computed from the merged satellite daily data (red line in Figure 1), representing the 80th percentile of SSS variability throughout the tropical North Atlantic (0–35°N). This means that the total variability in the region bounded by this contour is in the top 20% of the variability observed throughout the entire tropical North Atlantic. The region extends from 0° to 23° N and from 75°W to west Africa with a narrow band of high SSS variability (20°–40°W, 5°–11°N) that can be attributed to the NECC and Inter-Tropical Convergence Zone (ITCZ; black contour in Figure 1). The black contour encloses the upper 20% of precipitation variability in the tropical North Atlantic. The low variability of SSS within the black contour and between 1° and 5°N implies that the impact of ITCZ precipitation on SSS is not as strong as the advection of low-salinity water by the NECC. To minimize the impact of the ITCZ on the plume variability and to simplify the salinity balance analysis in the plume region, we define the plume region to be within the red rectangle in Figure 1 (70°W–42°W, 0°N–23°N). The plume index in this study is therefore defined as the spatial mean of SSS over the rectangle.

2.3. Impacts of Different Forcings

Potential forcings that affect interannual variability of the Amazon-Orinoco plume include river discharge (R), local evaporation (E) and precipitation (P), horizontal advection (adv), and vertical mixing. Previous studies (Dong et al., 2009; Ren et al., 2011) often use a salinity budget equation to attribute interannual variability of

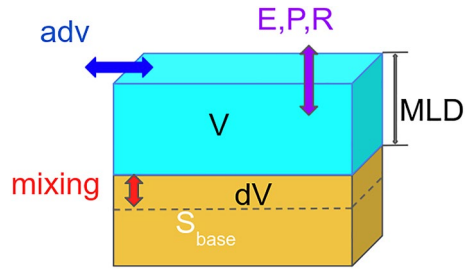


Figure 2. Simplified mixed layer salinity model.

mixed layer salinity to different components, such as fresh water flux, horizontal advection, vertical velocity induced by Ekman pumping, and diffusivity. However, because those terms include the synergy effects between different forcings, the contribution from each term is not due purely to the forcing of consideration. For example, the impacts of the surface freshwater flux on mixed layer salinity ($[E-P]S/h$, where E , P , S , and h are evaporation, precipitation, mixed layer salinity, and mixed layer depth, respectively) are proportional not only to the variability of the freshwater flux but also to the variability of the mixed layer depth, which is controlled by vertical entrainment mixing, and to the observed mixed layer salinity, which is controlled by all forcings. In this study, we assess the impact of each forcing on the plume SSS interannual variability using simple mixed layer salinity balances in which only one forcing at a time varies interannually.

Consider the plume as a box with fixed horizontal boundaries (the red rectangle in Figure 1) and a flexible bottom boundary that varies spatially and temporally with the mixed layer depth (Figure 2). Exchanges of water and salt through the surface and the lateral and bottom boundaries will result in an increase or decrease in the average mixed layer salinity. Since salinity is approximately constant vertically within the mixed layer, mean changes in salinity over the whole volume of the box are representative of changes in the spatial-mean SSS.

Different sensitivity analyses are conducted for different forcings to assess their partial impacts on the plume SSS. In a sensitivity analysis, only the forcing of consideration and the plume SSS can vary interannually; other background conditions, including the plume volume and salinity at the base of the plume, which represent the impacts of all available forcings, are set to their climatological values. Consider that at time t , the mixed layer (Figure 2) has volume \widehat{V}_c (in m^3), salinity \widehat{S} , and a total salt mass of $\widehat{V}_c\widehat{S}$ (in kg). The salinity balance at $t + dt$ due to forcing F , with other forcings and background volume V_c remaining climatological, can be formulated as

$$S_F = \frac{\widehat{V}_c\widehat{S}_F}{V_c} + \frac{dM_c}{V_c} + \frac{dM_{Fa}}{V_c} \quad (1)$$

where S_F and \widehat{S}_F are the mixed layer salinity at time $(t + dt)$ and (t) , respectively. The initial value of \widehat{S}_F at $t = 0$ is the actual plume SSS in January 2004. $\widehat{V}_c\widehat{S}_F$ represents the amount of salt in the mixed layer at time (t) , $dM_c = V_c S_c - \widehat{V}_c\widehat{S}_c$ represents the net change of salt mass due to all climatological forcings, including F , from (t) to $(t + dt)$, and dM_{Fa} represents the net change of salt mass due to anomalous F from (t) to $(t + dt)$. When F is purely climatological, the third term on the right side of Equation 1 is zero, and Equation 1 reduces to

$$S_{B(F)} = \frac{\widehat{V}_c\widehat{S}_F}{V_c} + \frac{dM_c}{V_c} \quad (2)$$

where $S_{B(F)} = S_F = S_c$ represents the climatological background variation of the mixed layer salinity. When F is not climatological, $S_{B(F)}$ contains the cumulative effects of anomalous F up to time (t) , and this is then the background condition for anomalous F at $(t + dt)$. The third term on the right hand of Equation 1 represents the effects of anomalous F at $(t + dt)$, which causes S_F to differ from $S_{B(F)}$.

For river forcing, the freshwater volume gained from anomalous river discharge of R_a increases the total volume of the plume box and raises the sea level. After equilibrium, the volume of water in the mixed layer does not change, leading to a loss of salt in the mixed layer of $R_a S_{B(R)}$ because the freshwater with zero salinity displaces the same volume of existing ocean water. Hence,

$$S_R = S_{B(R)} - \frac{R_a S_{B(R)}}{V_c} \quad (3)$$

This effect is easy to imagine when the anomalous river discharge is positive. When it is negative, the formula is the same because Equation 3 is an adjustment to the climatological river discharge that is already accounted for in the background salinity $S_{B(R)}$ (Equation 2).

Similarly for precipitation:

$$S_p = S_{B(P)} - \frac{P_a S_{B(P)}}{V_c} \quad (4)$$

For evaporation, freshwater lost due to evaporation E_a on the surface decreases the thickness of the mixed layer. Constant vertical entrainment mixing (i.e., the mixed layer volume) then introduces water at the base of the mixed layer with climatological salinity S_{bc} with a salt gain of $S_{bc}E_a$, hence

$$S_E = S_{B(E)} + \frac{E_a S_{bc}}{V_c} \quad (5)$$

For advection, changes in circulation can result in convergence or divergence inside the plume region, which can change both the total salt mass and volume of the plume box. Given net advected volume anomaly of V_{Ha} and net advected salt mass anomaly of M_{Ha} , if there is convergence in volume ($V_{Ha} > 0$), after equilibrium, the excessive volume is displaced from the mixed layer so that the salinity advected is the background salinity $S_{B(H)}$:

$$S_H = S_{B(H)} + \frac{-V_{Ha} S_{B(H)} + M_{Ha}}{V_c} \quad (6a)$$

In contrast, if there is volume divergence ($V_{Ha} < 0$), entrainment will introduce base water S_{bc} into the mixed layer:

$$S_H = S_{B(H)} + \frac{-V_{Ha} S_{bc} + M_{Ha}}{V_c} \quad (6b)$$

where V_H and M_H are the integrated net volume and salinity flux (kg month^{-1}), respectively, along the boundary of the plume region:

$$V_H = \int_W u h_c dy - \int_E u h_c dy + \int_S v h_c dx - \int_N v h_c dx \quad (7a)$$

and

$$M_H = \int_W u h_c S_c dy - \int_E u h_c S_c dy + \int_S v h_c S_c dx - \int_N v h_c S_c dx \quad (7b)$$

where u, v are surface zonal and meridional velocity, respectively, and h_c, S_c are the climatological mixed layer depth and sea surface salinity along the boundary, respectively. By fixing the mixed layer depth and sea surface salinity along the boundary at their climatological values, interannual variability of advection in the plume region is purely due to the variability of surface currents, avoiding the impacts of vertical mixing, precipitation, river discharge, and evaporation outside the plume region on the advection term.

Vertical (diapycnal) mixing is related to the rate of change of the mixed layer depth, which can be due to wind-induced turbulent mixing, current shear, buoyancy forcing, or horizontal advection of the mixed layer depth. The first three processes entrain subsurface water with different salinity relative to the surface layer and are therefore capable of changing the mixed layer salinity. The advection of shallower mixed layer depth into the plume region may also trigger vertical mixing if, for instance, wind-induced mixing in the plume region remains the same. Hence, changes of volume and salinity at the base of the mixed layer from (t) to $(t + dt)$ control variations of the plume salinity, not the volume anomaly compared to climatological volume:

$$S_z = \frac{\widehat{V} S_z + S_{bc} dV}{V} \text{ if } dV > 0 \quad (8a)$$

$$S_z = \hat{S}_z \text{ if } dV \leq 0 \quad (8b)$$

with $dV = V - \widehat{V}$.

Vertical velocity induced by horizontal divergence/convergence due to Ekman pumping or other processes is not included in the vertical mixing component. In the absence of turbulent mixing, vertical velocity (upwelling/downwelling) only raises or deepens the pycnocline, which changes the mixed layer depth locally without changing the

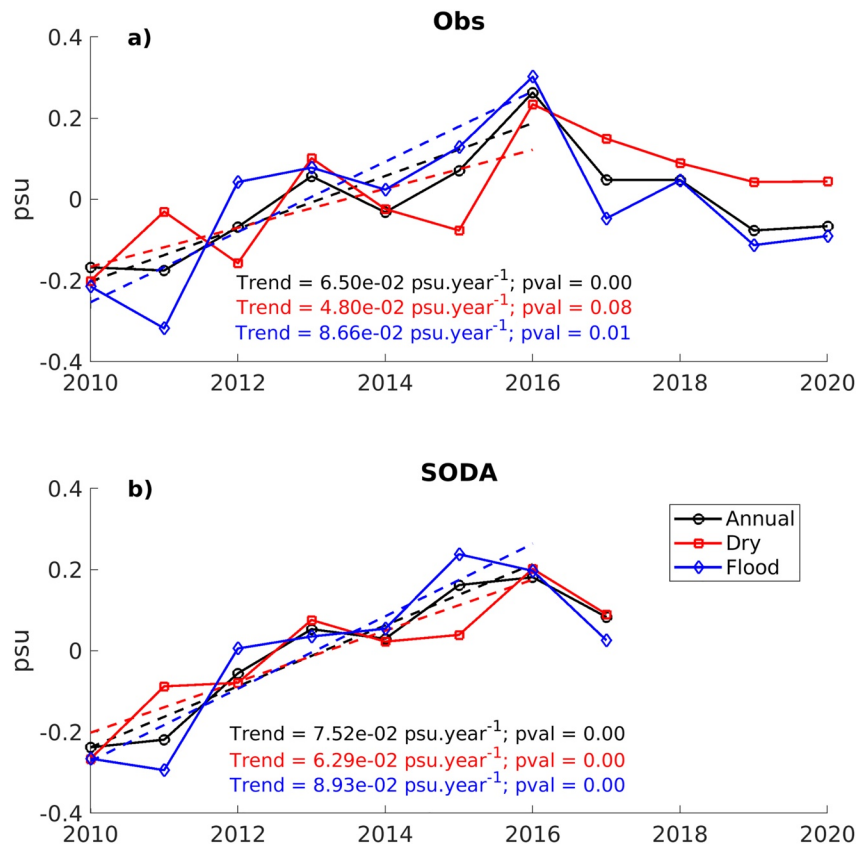


Figure 3. Interannual variability of Amazon-Orinoco plume sea surface salinity (SSS) (averaged over the red rectangle in Figure 1) from the merged satellite SSS data set (a) and the Simple Ocean Data Assimilation (SODA) reanalysis (b). Dry season is from January to March, and the flood season is from July to September, chosen based on climatological mean plume salinity (see Figure S2 in Supporting Information S1). The trends are computed over the period 2010–2016.

mixed layer salinity. In reality, if the vertical mixing length is deeper than the raised mixed layer in the upwelled water region, the upwelled water can be mixed up to the mixed layer and can affect the mixed layer salinity. Here, this term is attributed to advection because it is the forcing that creates the potential for a change in mixed layer salinity, and vertical mixing can act on that potential. In our simulations for forcings other than vertical mixing, we assume that vertical mixing is climatological and is constant for a given time step. Therefore, upwelled water is always introduced to the mixed layer and downwelling does not affect mixed layer salinity.

We limit these analyses to the Argo period from 2004 to 2017 when SODA benefits from the assimilation of more observations. The data and the time step dt used in these sensitivity analyses are monthly.

3. Results

3.1. Interannual Variability of SSS in the Plume Region

The Amazon-Orinoco plume exhibits strong interannual variability with a range in the annual mean plume SSS anomaly of -0.17 psu in 2010 to 0.26 psu in 2016 based on satellite data (black solid line in Figure 3a). The interannual range is similar in SODA with a minimum annual mean of -0.24 psu in 2010 and maximum annual mean of 0.18 psu in 2016. The discrepancies in the values between observations and SODA may be partly due to the fact that SODA does not assimilate satellite SSS. To put these values into perspective, the interannual range of SSS anomalies to the northeast of the plume region (the white rectangle in Figure 1) is about three to four times smaller: -0.07 to 0.09 from observations and -0.06 to 0.07 from the SODA reanalysis (Figure S3 in Supporting Information S1). These differences in the varying ranges between the plume and non-plume regions, confirmed

by both satellite observations and reanalysis, may illustrate the important role of river discharge and strong ocean dynamics in the plume region.

In some years, the plume SSS has similar anomalies in the flood and dry seasons, for example, 2010 and 2016 (Figures 3a and 3b). In other years, such as 2012 and 2015, the plume SSS has a reduced annual cycle of SSS with higher than normal salinity in the flood season and lower salinity in the dry season. In contrast, during 2011, the plume SSS has an amplified annual cycle with lower SSS in the flood season and higher SSS in the dry season. The correlation between observed plume SSS anomalies in the dry and flood seasons over the period 2010–2020 is only 0.48 and is not significant. These differences in the phases of wet and dry season SSS suggest that either the magnitude or type of forces that drive the plume SSS interannual variability is not the same throughout the year.

There are also significantly increasing trends in plume SSS of 0.89 and 0.75 psu per decade for the wet season and annual mean, respectively, during 2010–2016 (Figure 3a). The plume SSS shows an increasing trend over the dry season of 0.48 psu per decade, which is significant at 90%. These trends are all significant at 99% in the SODA reanalysis (Figure 3b).

3.2. Mechanisms of the Variability

To investigate the causes of interannual variability of the plume SSS, we look at the forcing variability in 2011 and 2015. These years represent amplified (2011) and reduced (2015) seasonal cycles of plume SSS that were observed in both observations and SODA (Figure 3).

Figure 4a shows that the mean plume SSS in the dry season (January–March) of the two years differs slightly (~ 0.1 psu), and this gap rapidly increases to about 0.45 psu in the flood season. Figure 4b–4f illustrates the potential forcings responsible for this variability of the plume SSS, including river discharge (R), precipitation (P), evaporation (E), horizontal advection by the ocean circulation (ADV, represented by zonal current Ucur), and vertical mixing using mixed layer depth as a proxy. The mixed layer depth shows a close relationship with the mean wind stress in the plume region (Figure 4b), highlighting the important role of wind-induced vertical mixing in the region (e.g., Rugg et al., 2016). Vertical mixing, advection, and precipitation have opposite signs between the years, reflecting a clear separation in their magnitudes (Figures 4b, 4c and 4e). Stronger precipitation and weaker vertical mixing (thinner mixed layer) support lower plume salinity in 2011 than in 2015. The positive anomaly of zonal current in 2011 (i.e., anomalous eastward flow) may represent a weakening of the NBC, NEC, and/or the strengthening of the NECC (Figure 1). This will be investigated later in this section. Evaporation and river discharge also show mirror-like patterns, but their magnitudes in the two years are mixed (Figures 4d and 4f).

Figure 5 shows the annual mean anomaly maps of the plume SSS and forcings in 2011 and 2015. In agreement with the spatial mean in Figure 4, the clear contrasts of salinity as well as wind stress, mixed layer depth, precipitation, and advection between the two years are seen almost everywhere in the plume region (Figures 5a–5h and 5). The wind stress fields in the two years are different not only in magnitude but also in the spatial patterns inside the plume region (Figures 5c and 5d). In 2011, southeasterly anomalous wind occurred over the northeastern part of the plume region, whereas west to southwesterly anomalous winds occupied the southwestern part. In contrast, strong northeasterly positive anomalous wind dominated the whole plume region in 2015. This strong northeasterly anomalous wind probably originated from the subtropical eastern Atlantic (Figure 5d). The mixed layer depth also shows close spatial variation with the wind stress field (Figures 5e–5f). The largest differences in plume salinity anomalies are in the southeastern portion of the plume box, where there is a large low-salinity patch in 2011 under weakened NBC, NEC (positive anomaly), and NECC (negative anomaly) conditions (Figures 5a and 5g). The weakening of the current systems may favor a more pronounced northward spreading of freshwater discharge originating near the equator since it allows the fresh water to stay within the plume region for a longer period of time. The shape of the large patch of low-salinity water is similar to that of the shallow mixed layer region (Figures 5a and 5e), suggesting that either weaker vertical mixing (thinner mixed layer) supported lower SSS or lower SSS created stronger stratification that limited mixing or both. In addition, this large low-SSS patch coincides with an area of lower than normal evaporation in 2011 and higher than normal evaporation in 2015 (Figures 5a, 5i and 5j). In the other parts of the plume, evaporation does not show large differences between the years. Precipitation also contributed to the low-salinity patch with higher than normal precipitation in 2011

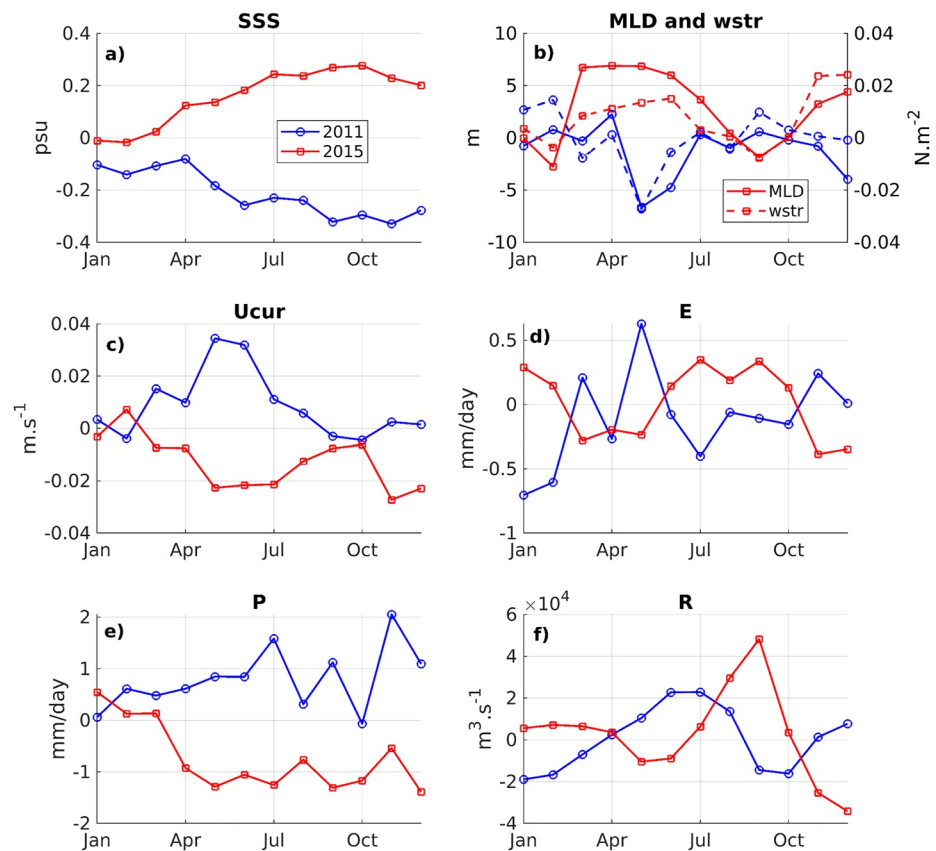


Figure 4. Annual cycles of spatially averaged forcings over the plume region for 2011 (blue lines) and 2015 (red lines). Shown are (a) sea surface salinity (SSS), (b) mixed layer depth (MLD, solid line) and wind stress (wstr, dashed line), (c) zonal current (Ucur), (d) evaporation (e), (e) precipitation (P), and (f) river discharge (R). All of the fields are from the Simple Ocean Data Assimilation data set.

and lower than normal precipitation in 2015 (Figures 5k and 5l). However, the strongest contrast of precipitation in the two years is in the northwestern part of the plume box.

All of the forcings except evaporation and river discharge contributed to the strong contrast in plume SSS between 2011 and 2015. However, it is unclear which forcings contributed most to the plume SSS variability. To quantify this, we evaluate the partial effect of each forcing on the plume SSS using the sensitivity analysis described in Section 2.3. The overall results of the analysis over the extended period from 2004 to 2017 (e.g., time series of each forcing term including the seasonal cycle) can be found in the supporting document (Figure S4 in Supporting Information S1).

Figure 6 illustrates the partial effects of the forcings on the plume SSS anomalies for the years 2011 and 2015. We can see that both evaporation and vertical mixing result in lower/higher plume salinity in 2011/2015 in agreement with the actual plume SSS variability in SODA (Figures 6a, 6e and 6f). However, the differences in these years caused by these forcings are minor compared to the SSS differences (Figure 6f). River discharge shows an opposite effect, contributing to higher plume salinity in 2011 compared to 2015 (Figure 6c) and thus, it cannot be the driver of the plume salinity contrast. Precipitation better reproduces the sign and magnitude of the plume SSS difference between the years with a plume salinity gap (2015 minus 2011) in the flood season (July–September) of about 0.25 psu, half of the actual value of ~0.50 psu. However, precipitation does not reproduce well the plume salinity gaps in the dry season (January–March) with a negative gap of about -0.10 psu predicted and 0.10 psu in SODA. Of all the forcings, advection best matches the actual plume salinity variation in SODA. It reproduces well (slightly larger) the plume salinity gaps in the dry (0.20 vs. 0.10 psu) and flood (0.60 vs. 0.50 psu) seasons. We also tested with another case study of 2010 versus 2016, which represents the minimum and maximum mean plume SSS anomaly, respectively. Advection is also the best match in terms of reproducing the magnitude of the

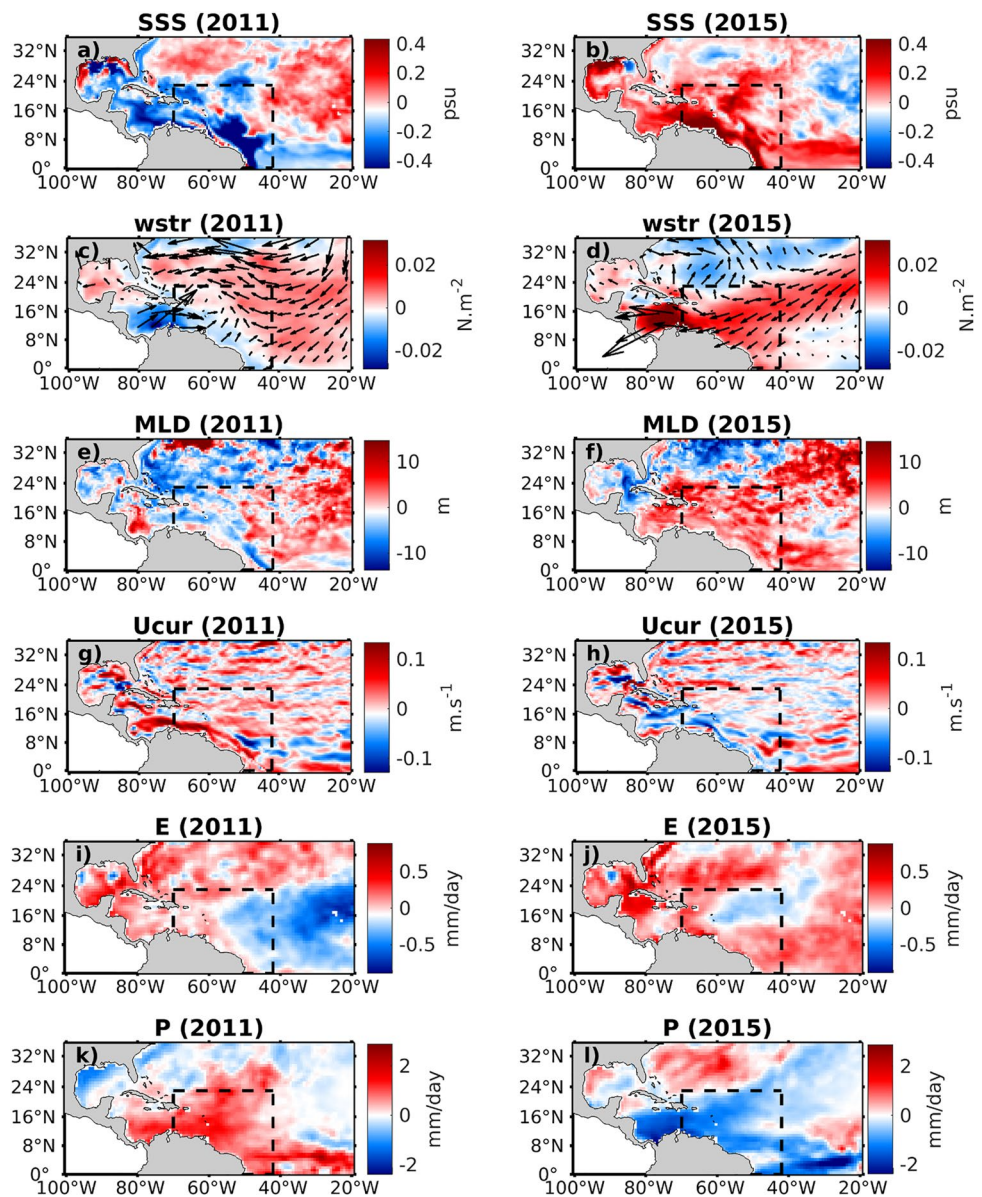


Figure 5. Comparisons of annual mean of anomalous forcings between 2011 and 2015: (a, b) sea surface salinity (SSS), (c, d) wind stress magnitude (shading) and vectors (arrows), (e, f) mixed layer depth (MLD), (g, h) zonal current (Ucur) with positive values indicating anomalously eastward current, (i, j) evaporation (E), and (k, l) precipitation (P). The dashed black rectangle represents the plume's influential region. All of the fields are from the Simple Ocean Data Assimilation data set.

difference in plume SSS (Figure S5 in Supporting Information S1) for those years. This converges to the findings of previous studies (Coles et al., 2013; Lentz, 1995) on the important role of advection for seasonal plume variability.

Table 1 summarizes the correlations between the SSS due to the different forcings and the actual plume SSS for different seasons over the extended period 2004–2017. It confirms the important role of advection for plume SSS interannual variability with significant positive correlations in all seasons ranging from 0.59 to 0.76. Figure 7 also shows that the partial effect of advection follows closely the actual variability of the plume SSS in SODA. Other forcings' effects either show insignificant (P) or even negative (R, mixing, E) correlations with the actual variability and thus cannot be the dominant forcing for the interannual variability of the Amazon-Orinoco plume SSS.

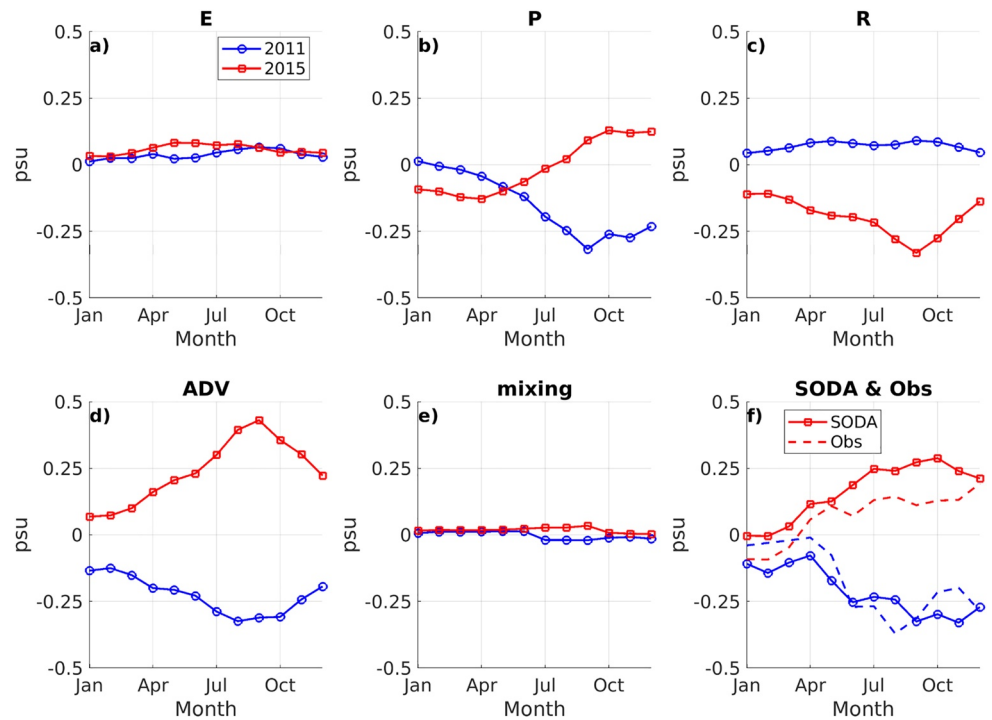


Figure 6. Spatial mean plume sea surface salinity anomalies due to different forcings (a–e) and from Simple Ocean Data Assimilation (SODA) and observations (f) for the year 2011 (blue lines) and 2015 (red lines).

Over the period 2004–2017, the plume salinity experienced a decreasing trend between 2004 and 2010 and an increase between 2010 and 2017 (black line in Figure 7). Although advection does not reproduce these phases perfectly, it is the only forcing that shows two distinguishable phases over the same periods. During the decreasing phase of 2004–2010, the plume SSS driven by advection has a decreasing trend of $-0.37 \text{ psu.decade}^{-1}$ (significant at the 95% level) compared to -0.62 for SSS in SODA. During the increasing phase of 2010–2017, the trends are 0.85 and $0.58 \text{ psu decade}^{-1}$ for the advection effect and SSS in SODA, respectively, all significant at the 95% level. None of the other forcings reproduces similar significant decreasing/increasing trends over the periods. This once again confirms the dominant role of advection in driving the plume SSS at interannual and decadal time scales.

3.3. Which Current System Is Most Important for Amazon-Orinoco Plume Variability?

We have seen that interannual and longer term variability of the Amazon-Orinoco plume SSS is strongly controlled by advection, and the dynamics in the plume region are complicated with the presence of three different major current systems, including the NBC, NEC, and NECC (Figure 1). Hence, the next question is: Which current system contributes most to the plume variability?

To answer this question, we first determine the lateral boundary of the plume region that is most important for the total net salinity flux. Figure 8a shows the interannual variability of the integrated salinity flux along different plume boundaries and the associated net flux computed using Equation 7. We can see that the salinity flux along the eastern boundary has the strongest variability and follows closely the net salinity flux. The correlation between the eastern boundary flux and the net flux is 0.63 , which is significant at 95%, whereas the fluxes along the other boundaries do not have significant

Table 1
Correlation Between Simulated Plume SSS Variability Under Impacts of Different Forcings and Actual Variability From SODA in Different Seasons Over the Period 2004–2017

	E	P	R	ADV	Mixing
Winter (1–3)	-0.23	0.06	-0.27	0.59	-0.66
Spring (4–6)	0.22	-0.04	-0.56	0.56	-0.17
Summer (7–9)	0.07	0.09	-0.44	0.58	-0.25
Fall (10–12)	-0.31	0.20	-0.25	0.76	-0.51
Annual	-0.09	0.12	-0.42	0.72	-0.45

Note. Bold values represent correlations with significance >95%.

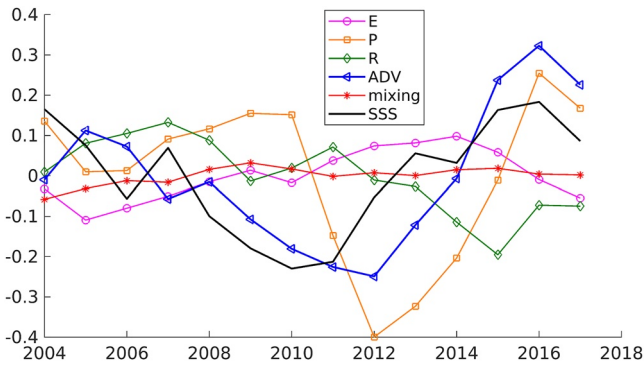


Figure 7. Interannual variability of simulated annual mean plume sea surface salinity (SSS) anomalies under impacts of different forcings and actual plume variability SSS from Simple Ocean Data Assimilation.

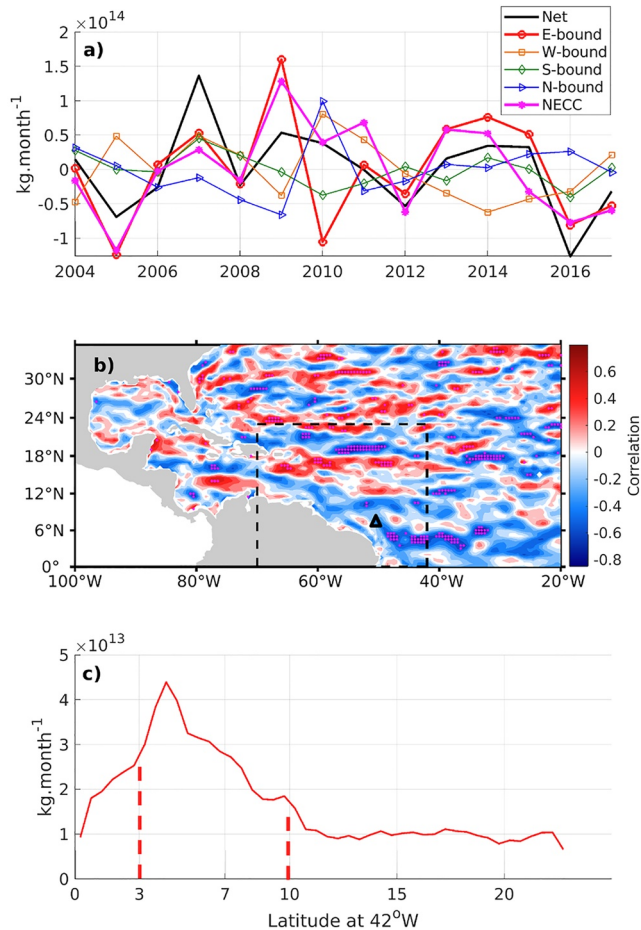


Figure 8. (a) Interannual variability of the integrated salinity flux (positive inward) along different boundaries of the plume region (black dashed rectangle) and associated net salinity flux, computed over 2004–2017 period. (b) Map of correlation between the net salinity flux anomalies and zonal current anomalies. Dotted regions show correlations significant at >95%. (c) Standard deviation of monthly anomalous salinity flux along the eastern boundary of the plume region.

correlations with the net flux. This remains true for climatological values: the eastern boundary flux provides the largest flux into the plume region and is the only component that has a significant correlation (0.83) with the net salinity flux (Figure S6a in Supporting Information S1). Therefore, the eastern boundary, which includes the variability of the NEC and NECC (Figure 1), is the most important source of variability for the mean Amazon-Orinoco plume SSS.

Next, we locate where in the eastern boundary the exchange of water and salt is most crucial to the net salinity flux. Figure 8b shows a correlation map between the horizontal salinity flux annual anomalies and zonal surface current annual anomalies computed over the 2004–2017 period. Along the eastern boundary of the plume, there is a region of highly significant correlations (at 95%) between 4° and 6° N. This is the region where the NECC is located (Garzoli & Katz, 1983; Richardson & Reverdin, 1987). The negative correlation in this region means that a stronger NECC results in a weaker net salinity flux (less salt advected into the region) since the NECC brings salt and water out of the plume region. This patch of significant correlations associated with the NECC stretches westward to the NBC retroflection at around 50° W and 8°N (the black triangle in Figure 8b). Note that the magnitude of the salt flux does not directly change the mean plume salinity, which also depends on the difference between the salinity of the water in the plume and at its boundaries. For example, if the salinity of the plume is the same as salinity outside the plume, the salt flux does not change the plume's salinity.

Figure 8c shows the variability (std) of the horizontal salinity flux along the eastern boundary with the highest interannual variability between 0° and 11°N. The actual latitude range of the NECC reported in previous studies (Garzoli & Katz, 1983; Richardson & Reverdin, 1987) is 3°–10°N (see also Figure S6c in Supporting Information S1). This range of latitudes contributes more than half of the total variability along the eastern boundary of the plume (Figure 8c). The integrated salinity flux along this range of latitudes of the NECC (the magenta line in Figure 8a) is also highly correlated with the eastern boundary flux and the total net salinity flux with coefficients of 0.75 and 0.68, respectively (significant at 99%). This means that the total variability of advection in the plume region is largely driven by the NECC. The NECC salt flux also has a significant correlation (95%) with the mean plume SSS anomalies of 0.58 over the 2004–2017 period. The positive correlation between NECC salt flux and the plume SSS means that a stronger NECC leads to higher plume SSS and conversely, a weaker NECC leads to lower plume SSS. This is probably due to the fact that the NECC tends to transport low-salinity water out of the plume region toward East Africa (Figure 1), reducing the residence time of low-salinity water inside the plume region.

3.4. The Role of Large-Scale Climate Phenomena

Although advection in general and the NECC in particular are the most influential forcing of the plume SSS interannual variability, advection can only explain about 50% of the total variance of the plume SSS annual mean anomalies (Table 1). The strong contrast between the plume SSS in 2011 and 2015 was associated with distinct differences not only in advection but also in precipitation, mixed layer depth, evaporation, and river discharge (Figure 4). This suggests that there is a large-scale driver behind these consistent changes in multiple forcings.

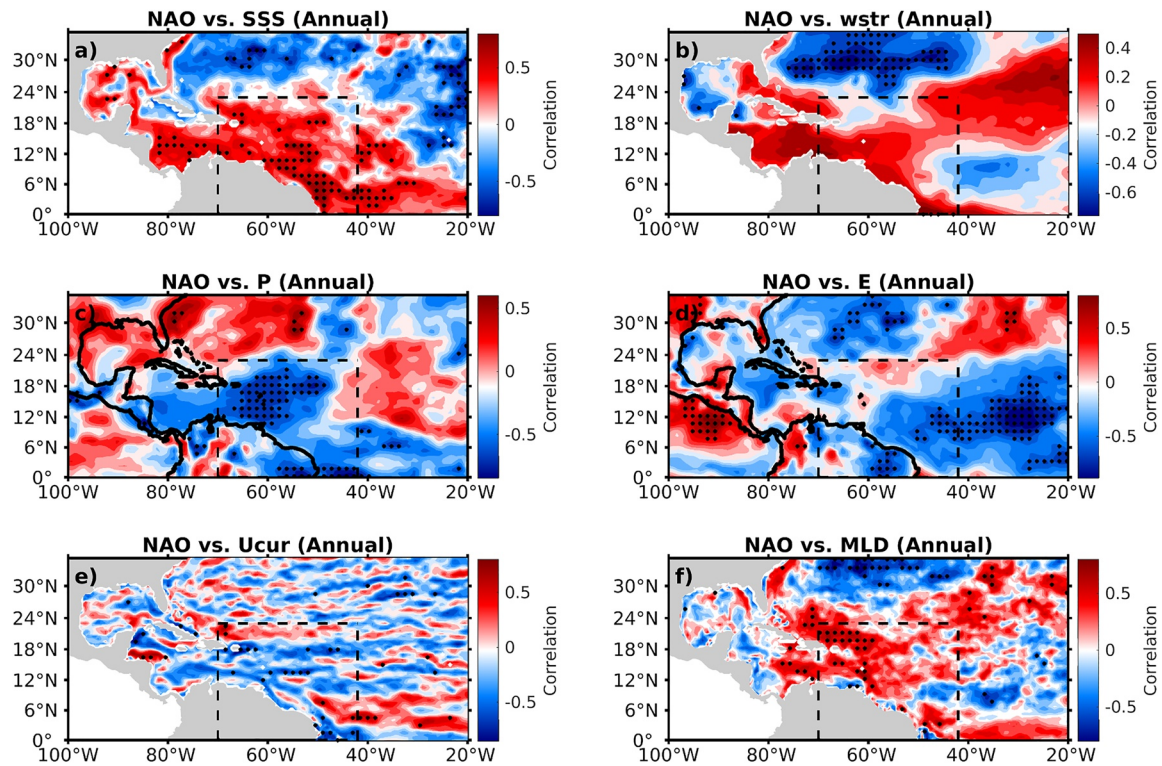


Figure 9. Correlation between winter (November–January) mean North Atlantic Oscillation (NAO) and annual mean of anomalous forcings in the following year. In (b), wind stress magnitude is used. Black dots represent regions of highly significant correlation (>95%).

Figure 9 shows correlation maps between the winter-time NAO index (November–January mean) and the annual means of anomalous forcings and plume SSS in the following year. First, over the plume region, the NAO has a positive correlation with wind stress (not highly significant, Figure 9b) and mixed layer depth (highly significant in the western part of the plume region, Figure 9e). The increase in mixed layer depth in the western basin is consistent with the signal found for negative phases of the Atlantic Meridional Mode (i.e., anomalously cold SST in the tropical North Atlantic relative to the South Atlantic) (Rugg et al., 2016). This means that a positive phase of the NAO (NAO+ hereafter) tends to increase the wind stress and mixed layer depth, which can potentially increase the plume SSS due to mixing with higher salinity at the base of the mixed layer. Second, NAO+ tends to decrease precipitation and evaporation over the Amazon–Orinoco catchment and plume region with highly significant negative correlations with precipitation and less significant negative correlations with evaporation (Figures 9c and 9d). This will result in increasing plume salinity because precipitation has much stronger variability than evaporation (Figures 4 and 6). Third, NAO+ tends to strengthen the westward NBC and NEC (negative correlation) and eastward NECC (positive correlation), which may also result in higher plume SSS because the strengthened current systems tend to reduce the residence time of low-salinity water in the plume region. Therefore, NAO + influences almost all forcings (except evaporation) in a way that increases the plume SSS (Figure 9a). The region of highly significant correlations between the NAO and plume SSS seems to coincide with the region of active NBC and NECC. Given the important role of advection revealed from previous results, this suggests that the largest impact of the NAO on the plume SSS is through advection.

Figures 10c and 10d show that ENSO has significant negative correlations with evaporation and less significant negative correlations with precipitation over the Amazon–Orinoco catchment and plume regions. These correlations suggest that El Niño tends to decrease evaporation and precipitation, probably resulting in higher plume salinity due to stronger impacts of precipitation on plume SSS (Figures 4 and 6). The impacts of ENSO on precipitation and evaporation are qualitatively similar to those of the NAO. However, the NAO shows stronger correlations with precipitation than ENSO and thus the NAO may play a larger role in driving plume SSS via the surface moisture flux than ENSO. ENSO has significant negative correlations with wind stress, but unlike the NAO, it has spatially varying correlations with mixed layer depth, meaning that the impact of ENSO on vertical mixing is

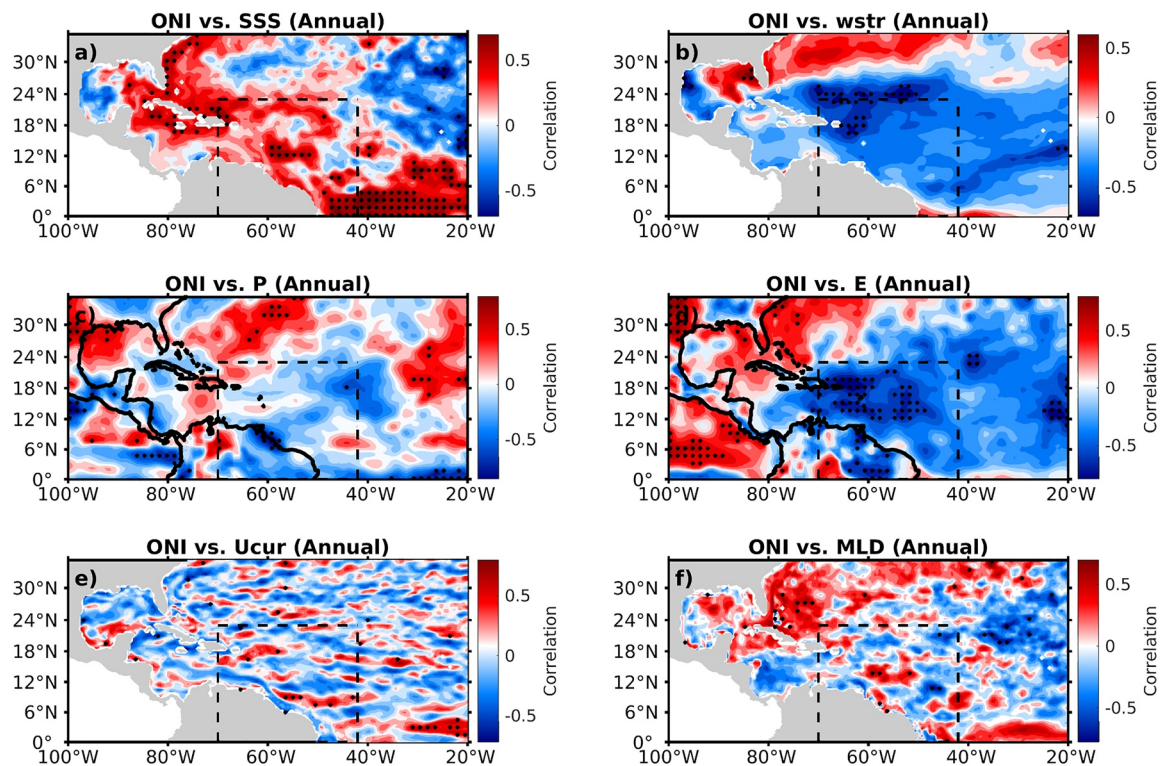


Figure 10. (a) Correlation between winter mean (November–January) Ocean Niño Index (ONI) and annual mean of anomalous forcings in the following year. In (b), wind stress magnitude is used. Black dots represent regions of highly significant correlation (>95%).

unclear. ENSO also has weak negative correlations with the NBC. Overall, ENSO has positive correlations with SSS over the plume region, meaning that El Niño tends to increase the plume SSS. However, ENSO's effects on the plume SSS are not as strong as the NAO's (Figures 9a vs. 10a).

To investigate the causes of the stronger influence of the NAO on plume SSS compared to ENSO, we consider seasonal and spatial variations of their correlations. Figures 11a and 11b show meridional migrations of the NAO's influence on wind stress and precipitation. The band of positive correlations between the NAO and wind stress is located outside the plume region in January (Figure 11a). This band migrates southward and reaches the equator in April. It then increases in magnitude until July and weakens in the following months. Similarly, the strong negative band of correlations between the NAO and precipitation starts in March outside the plume region (Figure 11b). This band migrates southward, reaches the upper plume region in April, and remains there until August before extending southward to the equator in October–November. These migrations of the NAO's effects on wind and rainfall result in the NAO's strongest influence on the forcing fields occurring over the plume region in the flood season (Figure S7 in Supporting Information S1). The lag of the NAO's effects on precipitation compared to wind stress needs further investigation. In contrast, there are strong negative bands of correlations between ONI and wind stress and precipitation over the plume region during the winter months (January–February, Figures 11c and 11d). These bands of correlation weaken in the following months. This means that it takes less time for ENSO's effects on the forcing fields to arrive in the plume region, and ENSO's strongest effects are observed in the dry season (Figure S8 in Supporting Information S1).

The seasonal differences between the NAO's and ENSO's effects on the forcing fields over the plume region may be due to differences in the locations of the centers of forcing of the NAO and ENSO in relation to the plume region. First, the Azores high, where NAO effects initiate, is farther away from the plume region than the western tropical pacific, where ENSO effects initiate. Second, zonal propagation in the atmosphere is generally much faster than meridional propagation because of equatorial waves. This difference in phasing of the impacts of the NAO and ENSO on the plume region may also partly explain the low correlation between the plume index in the flood season and the dry season (Section 3.1, Figure 3).

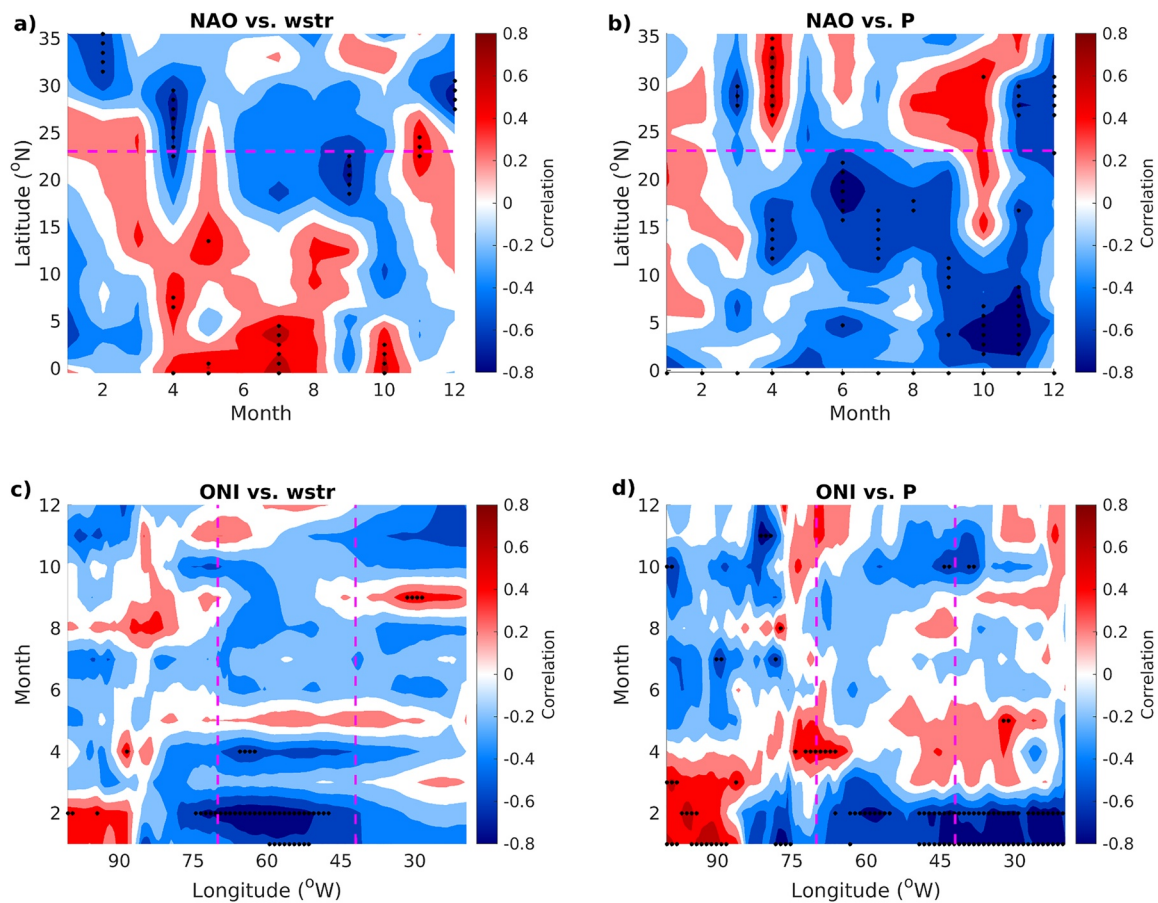


Figure 11. Hovmöller maps of correlations between climate indexes (North Atlantic Oscillation [NAO], Ocean Niño Index [ONI]) and wind stress magnitude (wstr) and precipitation (P). Both wind stress magnitude and precipitation are zonally averaged over the plume longitudes (70° W– 42° W) and meridionally averaged over the plume latitudes (0° N– 23° N) when computing correlations with NAO (a, b) and ONI (c, d), respectively. The magenta horizontal and vertical dashed lines indicate the plume meridional and zonal boundaries. Black dots represent regions of highly significant correlations (> 95%).

Figure 12 confirms the positive relationship between the NAO and plume SSS and between ONI and plume SSS. We also see contrasting magnitudes of the indices in the case studies of 2011 and 2015. The year 2011 followed a winter of strong negative NAO (NAO–) and La Niña, resulting in stronger precipitation over both the Amazon-Orinoco catchment and plume region, weaker wind stress, and weaker advection. These conditions together resulted in a low plume SSS year. A contrasting climate condition was present in the winter of 2014–2015 with a positive phase of the NAO and a strong El Niño. These conditions resulted in lower precipitation and river discharge and stronger advection, which increased plume SSS in that year. The extreme positive phases of the NAO and ENSO in the winter of 2015–2016 also explain the occurrence of the highest plume SSS anomalies of the period in 2016. Observed plume SSS also peaked in 2016 and then decreased in response to decreasing phases of the NAO and ENSO during 2016–2020. Over the period 2004–2017, the correlation between the NAO and SODA plume SSS is 0.70, which is significant at 99%, whereas the overall correlation between ONI and SODA plume SSS is 0.51 and less significant (at 90%). The respective correlations between observed plume SSS and NAO and ONI indices over the 2010–2020 period are 0.60 (95% significance) and 0.43 (not significant). This once again confirms a stronger influence of the NAO on Amazon-Orinoco plume variability.

4. Discussion and Conclusions

In this study, we characterize the plume variability using mean SSS over a fixed plume region (Figure 1). Previous studies characterized the plume variability using plume size computed based on the area of water with SSS less than certain criteria (Fournier et al., 2017; Grodsky et al., 2014; Molleri et al., 2010; Zeng et al., 2008). To

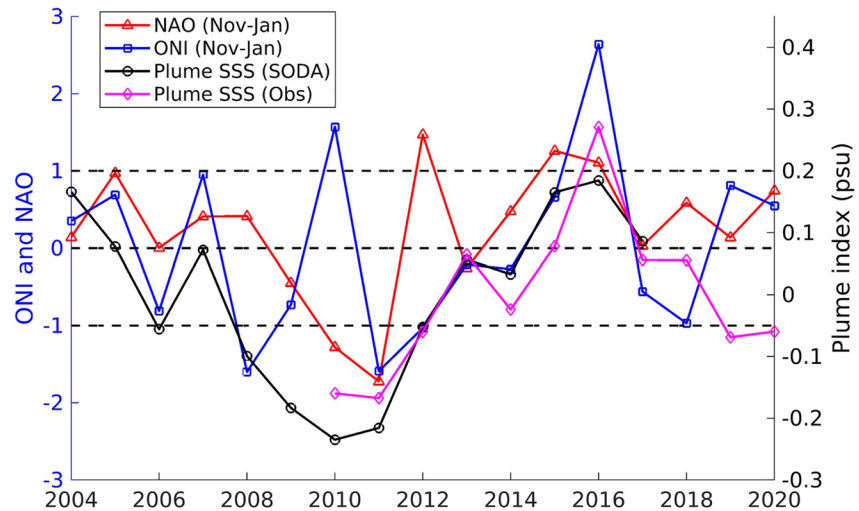


Figure 12. Interannual variation of climate indices and annual mean plume sea surface salinity (SSS) anomalies from Simple Ocean Data Assimilation (SODA) and observations.

test how close these area-averaged SSS and plume size indices are, we computed plume size with both satellite and SODA SSS using similar plume size criteria as in Fournier et al., 2017 (SSS < 35.5 psu). We found that the two indices are closely related with correlations of -0.84 and -0.69 for monthly climatological and interannual anomalies, respectively, using satellite SSS over the 2010–2020 period (Figure S9 in Supporting Information S1). The correlations found using SODA SSS over the 2004–2017 period are also high: -0.85 and -0.93 for monthly climatological and interannual anomalies, respectively. This means that there is little difference between the two indices.

Some studies highlighted the important role of river discharge for plume size seasonal variations (Molleri et al., 2010; Zeng et al., 2008). We also found highly significant seasonal correlations between Amazon-Orinoco river discharge and plume size from satellite and SODA with coefficients of 0.95 and 0.94, respectively, when plume size lags by 3 months, in agreement with those studies (Figure S10 in Supporting Information S1). This means that river discharge is the dominant driver of seasonal variability of the Amazon-Orinoco plume. However, on interannual time scales, the correlations between river discharge and plume size anomalies are low and insignificant with correlations of 0.25 and 0.16 based on satellite and SODA SSS, respectively. This suggests a minor influence of river discharge on interannual variability of the Amazon-Orinoco plume. However, other studies (e.g., Grodsky & Carton, 2018) have pointed out the importance of southern tributaries in conveying NAO effects to the interannual variability of the Amazon system discharge. Since it is still challenging for ocean reanalyses including SODA to accurately account for the effects of continental runoff due to limited observations, the role of river discharge on the Amazon-Orinoco plume interannual variability may have been underestimated. However, given the similarities of interannual variability of the plume SSS from SODA and satellite data (Figure 3), SODA has reasonably reproduced the actual interannual variability of the plume SSS. This means that the missing runoff from the southern tributaries is unlikely to be important for the total variability of the plume SSS.

We conducted sensitivity analyses to compare the impacts of individual forcing on the plume SSS interannual variability and long-term tendency. In doing these tests, we ignored the synergy effect (interactions) among different forcings, which may result in underestimation or overestimation of the impacts of each forcing term. Further studies will be helpful for quantifying in more detail the contributions of different forcings to the interannual variability and trends of the plume SSS.

Using satellite observations of sea surface salinity, we showed strong interannual variability of the Amazon-Orinoco plume over the period 2010–2020 with a magnitude that is about five times larger than the surrounding region. This interannual variability of the plume SSS was found to be well reproduced in the SODA reanalysis. Using data from the SODA reanalysis and its forcings over an extended period from 2004 to 2017, we found that horizontal advection was the most important forcing of the interannual variability of the plume SSS. Exchange of

water along the eastern boundary, especially within the active latitude range of the NECC, is most crucial to the variability of the advected net salinity flux and the plume SSS.

The variability of the forcings in the period was found to be strongly related to the NAO and ENSO. Over the plume region, the NAO appeared to be most influential on the forcing fields in the flood season, whereas ENSO had a stronger influence on the forcing fields in the dry season. These results identify NAO as the dominant driver of the plume SSS through its modulations of precipitation, vertical mixing, and especially horizontal advection. The difference in seasonality of the NAO's and ENSO's impact on the plume region partly explains the different variability of the plume SSS in the flood and dry seasons. The plume SSS also shows a significant upward trend during 2010–2016 as both the NAO and ENSO transitioned from a negative to a positive phase. It then shows a downtrend during 2017–2020 when both the NAO and ENSO are in decreasing phases. Under global warming, a possible increase in the magnitude and change in position of the NAO (Hu & Wu, 2004), combined with an increase in the frequency of extreme ENSO events (Cai et al., 2014), may result in an increase in the magnitude and a change in the phases of seasonal, interannual, and decadal variations of Amazon-Orinoco plume salinity with potential impacts on ocean-atmosphere interaction and biogeochemistry (Gevaudan et al., 2021; Subramaniam et al., 2008).

Data Availability Statement

All data used in this study are available publicly from the following websites: ESA CCI monthly SSS data, version v03.21: https://data.ceda.ac.uk/neodc/esacci/sea_surface_salinity/data/; SODA data: <https://www.soda.umd.edu/>; ERA-Interim data: <https://apps.ecmwf.int/>; HYBAM data: <http://hybam.omp.obs-mip.fr/>; ENSO and NAO climate indices: <https://psl.noaa.gov/>.

References

- Berrisford, P., Dee, D., Poli, P., Brugge, R., Fielding, K., Fuentes, M., et al. (2011). The ERA-Interim archive Version 2.0, Shinfield Park. *Reading, 1*, 23.
- Cai, W., Borlace, S., Lengaigne, M., van Rensch, P., Collins, M., Vecchi, G., et al. (2014). Increasing frequency of extreme El Niño events due to greenhouse warming. *Nature Climate Change*, *4*, 111–116. <https://doi.org/10.1038/NCLIMATE2100>
- Carton, J. A., Chepurin, G. A., & Chen, L. (2018). SODA3: A new ocean climate reanalysis. *Journal of Climate*, *31*, 6967–6983. <https://doi.org/10.1175/jcli-d-18-0149.1>
- Chérubin, L. M., & Richardson, P. L. (2007). Caribbean current variability and the influence of the Amazon and Orinoco freshwater plumes. *Deep Sea Research Part 1: Oceanographic Research Papers*, *54*(9), 1451–1473. <https://doi.org/10.1016/j.dsr.2007.04.021>
- Coles, V. J., Brooks, M. T., Hopkins, J., Stukel, M. R., Yager, P. L., & Hood, R. R. (2013). The pathways and properties of the Amazon River plume in the Tropical North Atlantic Ocean. *Journal of Geophysical Research: Oceans*, *118*(12), 6894–6913. <https://doi.org/10.1002/2013JC008981>
- Czaja, A., van der Vaart, P., & Marshall, J. (2002). A diagnostic study of the role of remote forcing in tropical Atlantic variability. *Journal of Climate*, *15*, 32802–33290. [https://doi.org/10.1175/1520-0442\(2002\)015<3280:adsot>2.0.co;2](https://doi.org/10.1175/1520-0442(2002)015<3280:adsot>2.0.co;2)
- Dong, S., Garzoli, S. L., & Baringer, M. (2009). An assessment of the seasonal mixed layer salinity budget in the Southern Ocean. *Journal of Geophysical Research*, *114*(C12). <https://doi.org/10.1029/2008JC005258>
- Enfield, D. B., & Mayer, D. A. (1997). Tropical Atlantic sea surface temperature variability and its relation to El Niño southern Oscillation. *Journal of Geophysical Research*, *102*(C1), 929–945. <https://doi.org/10.1029/96JC03296>
- Foltz, G. R., Grodsky, S. A., Carton, J. A., & McPhaden, M. J. (2004). Seasonal salt budget of the northwestern tropical Atlantic Ocean along 38°W. *Journal of Geophysical Research*, *109*(C3), C03052. <https://doi.org/10.1029/2003JC002111>
- Foltz, G. R., Schmid, C., & Lumpkin, R. (2015). Transport of surface freshwater from the equatorial to the subtropical North Atlantic ocean. *Journal of Physical Oceanography*, *45*(4), 1086–1102. <https://doi.org/10.1175/JPO-D-14-0189.1>
- Fournier, S., Vandemark, D., Gaultier, L., Lee, T., Jonsson, B., & Gierach, M. M. (2017). Interannual variation in Offshore advection of Amazon-Orinoco plume waters: Observations, forcing mechanisms, and impacts. *Journal of Geophysical Research: Oceans*, *122*(11), 8966–8982. <https://doi.org/10.1002/2017JC013103>
- Garzoli, S. L., & Katz, E. J. (1983). The forced annual Reversal of the Atlantic North Equatorial countercurrent. *Journal of Physical Oceanography*, *13*(11), 2082–22090. [https://doi.org/10.1175/1520-0485\(1983\)013<2082:tfarot>2.0.co;2](https://doi.org/10.1175/1520-0485(1983)013<2082:tfarot>2.0.co;2)
- George, S. E., & Saunders, M. A. (2001). North Atlantic Oscillation impact on tropical North Atlantic winter atmospheric variability. *Geophysical Research Letters*, *28*(6), 1015–1018. <https://doi.org/10.1029/2000GL012449>
- Gevaudan, M., Jouanno, J., Durand, F., Morvan, G., Renault, L., & Samson, G. (2021). Influence of ocean salinity stratification on the tropical Atlantic Ocean surface. *Climate Dynamics*, *57*, 321–340. <https://doi.org/10.1007/s00382-021-05713-z>
- Giffard, P., Llovel, W., Jouanno, J., Morvan, G., & Decharme, B. (2019). Contribution of the Amazon River discharge to regional sea level in the tropical Atlantic Ocean. *Water*, *11*(11), 2348. <https://doi.org/10.3390/w11112348>
- Gouveia, N. A., Gherardi, D. F. M., Wagner, F. H., Paes, E. T., Coles, V. J., & Aragão, L. E. O. C. (2019). The salinity structure of the Amazon River plume drives spatiotemporal variation of oceanic primary productivity. *Journal of Geophysical Research: Biogeosciences*, *124*(1), 147–165. <https://doi.org/10.1029/2018JG004665>
- Grodsky, S. A., & Carton, J. A. (2018). Delayed and quasi-synchronous response of tropical Atlantic surface salinity to rainfall. *Journal of Geophysical Research: Oceans*, *123*(8), 5971–5985. <https://doi.org/10.1029/2018JC013915>
- Grodsky, S. A., Reverdin, G., Carton, J. A., & Coles, V. J. (2014). Year-to-year salinity changes in the Amazon plume: Contrasting 2011 and 2012 Aquarius/SACD and SMOS satellite data. *Remote Sensing of Environment*, *140*, 14–22. <https://doi.org/10.1016/j.rse.2013.08.033>

Acknowledgments

GRF was supported by the Climate Variability and Predictability (CVP) Program of NOAA's Climate Program Office and base funds to AOML's Physical Oceanography Division. NDD acknowledges support from the Department of Oceanography, Faculty of Hydrology Meteorology and Oceanography, VNU University of Science.

- Hu, C., Montgomery, E., Schmitt, R., & Mullerkarger, F. (2004). The dispersal of the Amazon and Orinoco river water in the tropical Atlantic and Caribbean Sea: Observation from space and S-PALACE floats. *Deep Sea Research Part II: Topical Studies in Oceanography*, 51(10–11), 1151–1171. [https://doi.org/10.1016/S0967-0645\(04\)00105-5](https://doi.org/10.1016/S0967-0645(04)00105-5)
- Hu, Z.-Z., & Wu, Z. (2004). The intensification and shift of the annual North Atlantic Oscillation in a global warming scenario simulation. *Tellus A: Dynamic Meteorology and Oceanography*, 56(2), 112–124. <https://doi.org/10.3402/tellusa.v56i2.14403>
- Hurrell, J. W., & Deser, C. (2010). North Atlantic climate variability: The role of the North Atlantic Oscillation. *Journal of Marine Systems*, 14. <https://doi.org/10.1016/j.jmarsys.2009.11.002>
- Lentz, S. J. (1995). Seasonal variations in the horizontal structure of the Amazon Plume inferred from historical hydrographic data. *Journal of Geophysical Research*, 100(C2), 2391. <https://doi.org/10.1029/94JC01847>
- Lopez, R., Lopez, J. M., Morell, J., Corredor, J. E., & Del Castillo, C. E. (2013). Influence of the Orinoco River on the primary production of eastern Caribbean surface waters. *Journal of Geophysical Research*, 118(9), 4617–4632. <https://doi.org/10.1002/jgrc.20342>
- Moller, G. S. F., Nnovo, E. M. L. D., & Kampel, M. (2010). Space-time variability of the Amazon River plume based on satellite ocean color. *Continental Shelf Research*, 30(3–4), 342–352. <https://doi.org/10.1016/j.csr.2009.11.015>
- Muller-Karger, F. E., McClain, C. R., & Richardson, P. L. (1988). The dispersal of the Amazon's water. *Nature*, 333(6168), 56–59. <https://doi.org/10.1038/333056a0>
- Ren, L., Speer, K., & Chassignet, E. P. (2011). The mixed layer salinity budget and sea ice in the Southern Ocean. *Journal of Geophysical Research*, 116(C8). <https://doi.org/10.1029/2010JC006634>
- Reverdin, G., Olivier, L., Foltz, G. R., Speich, S., Karstensen, J., Horstmann, J., et al. (2021). Formation and evolution of a freshwater plume in the northwestern tropical Atlantic in February 2020. *Journal of Geophysical Research: Oceans*. <https://doi.org/10.1029/2020JC016981>
- Richardson, P. L., & Reverdin, G. (1987). Seasonal cycle of velocity in the Atlantic North Equatorial Countercurrent as measured by surface drifters, current meters, and ship drifts. *Journal of Geophysical Research*, 92(C4), 3691. <https://doi.org/10.1029/jc092ic04p03691>
- Ropelewski, C. F., & Halpert, M. S. (1987). Global and regional scale precipitation patterns associated with the El Niño/southern Oscillation. *Monthly Weather Review*, 115(8), 1606–1626. [https://doi.org/10.1175/1520-0493\(1987\)115<1606:garspp>2.0.co;2.CO;2](https://doi.org/10.1175/1520-0493(1987)115<1606:garspp>2.0.co;2.CO;2)
- Rugg, A., Foltz, G. R., & Perez, R. C. (2016). Role of mixed layer dynamics in tropical North Atlantic interannual sea surface temperature variability. *Journal of Climate*, 29, 8083–8101. <https://doi.org/10.1175/jcli-d-15-0867.1>
- Subramaniam, A., Yager, P. L., Carpenter, E. J., Mahaffey, C., Björkman, K., Cooley, S., et al. (2008). Amazon River enhances diazotrophy and carbon sequestration in the tropical North Atlantic Ocean. *Proceedings of the National Academy of Sciences*, 105, 10460–10465. <https://doi.org/10.1073/pnas.0710279105>
- Tyaquicã, P., Veleda, D., Lefèvre, N., Araujo, M., Noriega, C., Caniaux, G., et al. (2017). Amazon plume salinity response to ocean teleconnections. *Frontiers in Marine Science*, 4. <https://doi.org/10.3389/fmars.2017.00250>
- Varona, H. L., Veleda, D., Silva, M., Cintra, M., & Araujo, M. (2019). Amazon River plume influence on Western Tropical Atlantic dynamic variability. *Dynamics of Atmospheres and Oceans*, 85, 1–15. <https://doi.org/10.1016/j.dynatmoce.2018.10.002>
- Vizy, E. K., & Cook, K. H. (2010). Influence of the Amazon/Orinoco plume on the summertime Atlantic climate. *Journal of Geophysical Research*, 115(D21). <https://doi.org/10.1029/2010JD014049>
- Zeng, N. (1999). Seasonal cycle and interannual variability in the Amazon hydrologic cycle. *Journal of Geophysical Research*, 104(D8), 9097–9106. <https://doi.org/10.1029/1998JD200088>
- Zeng, N., Yoon, J.-H., Marengo, J. A., Subramaniam, A., Nobre, C. A., Mariotti, A., & Neelin, J. D. (2008). Causes and impacts of the 2005 Amazon drought. *Environmental Research Letters*, 3(1), 014002. <https://doi.org/10.1088/1748-9326/3/1/014002>